Icarus 208 (2010) 468–481

Contents lists available at ScienceDirect

Icarus

journal homepage: www.elsevier.com/locate/icarus

Numerical modelling of heating in porous planetesimal collisions

T.M. Davison [a,*], G.S. Collins [a], F.J. Ciesla [b]

[a] Impacts and Astromaterials Research Centre, Department of Earth Science and Engineering, Imperial College London, SW7 2AZ, United Kingdom
[b] Department of the Geophysical Sciences, The University of Chicago, 5734 South Ellis Avenue, Chicago, IL 60430, USA

ARTICLE INFO

Article history:
Received 1 May 2009
Revised 6 January 2010
Accepted 31 January 2010
Available online 10 February 2010

Keywords:
Collisional physics
Impact processes
Planetary formation
Planetesimals

ABSTRACT

Collisions between planetesimals at speeds of several kilometres per second were common during the early evolution of our Solar System. However, the collateral effects of these collisions are not well understood. In this paper, we quantify the efficiency of heating during high-velocity collisions between planetesimals using hydrocode modelling. We conducted a series of simulations to test the effect on shock heating of the initial porosity and temperature of the planetesimals, the relative velocity of the collision and the relative size of the two colliding bodies. Our results show that while heating is minor in collisions between non-porous planetesimals at impact velocities below 10 km s^{-1}, in agreement with previous work, much higher temperatures are reached in collisions between porous planetesimals. For example, collisions between nearly equal-sized, porous planetesimals can melt all, or nearly all, of the mass of the bodies at collision velocities below 7 km s^{-1}. For collisions of small bodies into larger ones, such as those with an impactor-to-target mass ratio below 0.1, significant localised heating occurs in the target body. At impact velocities as low as 5 km s^{-1}, the mass of melt will be nearly double the mass of the impactor, and the mass of material shock heated by 100 K will be nearly 10 times the mass of the impactor. We present a first-order estimate of the cumulative effects of impact heating on a porous planetesimal parent body by simulating the impact of a population of small bodies until a disruptive event occurs. Before disruption, impact heating is volumetrically minor and highly localised; in no case was more than about 3% of the parent body heated by more than 100 K. However, heating during the final disruptive collision can be significant; in about 10% of cases, almost all of the parent body is heated to 700 K (from an initial temperature of ~300 K) and more than a tenth of the parent body mass is melted. Hence, energetic collisions between planetesimals could have had important effects on the thermal evolution of primitive materials in the early Solar System.

1. Introduction

Many meteorites we observe, and hence the asteroid parent body they are derived from, have been heated—expressed, for example, as areas of melt, thermal metamorphism, and differentiation, most of which occurred during the first few million years of our Solar System's formation. More than 90% of all meteorite falls on Earth have experienced a degree of melting or metamorphism (Rubin, 1995). The source of this heating has long been an area of uncertainty in planetary science, with many different hypotheses being suggested. Electromagnetic induction was proposed to have played a role (e.g., Sonett et al., 1968; Herbert, 1989); though, as reviewed by Ghosh et al. (2006), is unlikely given that the needed solar wind flux through the plane of the Solar System was likely very small. On the other hand, short-lived radio-nuclides, in particular ^{26}Al (Urey, 1955; Lee et al., 1976; MacPherson et al., 1995; Russell et al., 1996; Srinivasan et al., 1999) have been shown to provide sufficient energy to cause both thermal metamorphism and differentiation of primitive bodies (e.g., Ghosh et al., 2006, and references therein).

An alternative source of heating that has been discussed over the years is shock heating in collisions or impacts between planetesimals—primitive solid bodies 1–100 km in diameter—during the early runaway growth period of Solar System evolution. According to standard models, rapid planetesimal growth formed Moon- to Mars-size planetary embryos throughout the inner Solar System during this time (Wetherill and Stewart, 1989), which probably lasted about 10 million years from the time that the first solid material in the Solar System was formed (Bottke et al., 2005). The terrestrial planets themselves are the products of energetic collisions between planetesimals and planetary embryos (Wetherill and Stewart, 1989). Further, there are a number of shock effects in meteorites best explained by the hypervelocity impact of planetesimals (e.g., Chao, 1967, 1968; Kieffer, 1971; Scott et al., 1992; Stöffler et al., 1991; Sharp and de Carli, 2006). It has even been suggested that the compaction and lithification of early planetesimals was the result of similar impacts (e.g., Scott, 2002; Consolmagno

* Corresponding author.
E-mail address: thomas.davison02@imperial.ac.uk (T.M. Davison).

0019-1035/$ - see front matter © 2010 Elsevier Inc. All rights reserved.
doi:10.1016/j.icarus.2010.01.034

and Britt, 2004). Given the energy and frequency of these events, many have suggested that planetesimal impacts may have contributed to the heating, and possible melting, of primitive bodies (Wasson et al., 1987; Cameron et al., 1990; Rubin, 1995).

Impacts have largely been dismissed as a source of substantial heating in asteroid thermal evolution, however, as previous models suggested that small-body collisions early in the Solar System were relatively inefficient at heating compared to the decay of short-lived radio-nuclides (e.g., Keil et al., 1997; McSween et al., 2002). In a comprehensive study combining observations from terrestrial craters, results from laboratory shock experiments, numerical modelling and theoretical considerations, Keil et al. (1997) critically examined impact heating in small-body collisions. In particular, they discussed results from Smooth Particle Hydrodynamics (SPH) simulations of collisions at 3–7 km s^{-1} between planetesimals 10–1000 km in diameter (Love and Ahrens, 1996). They concluded that while some amount of localised melting and heating occurred, the low surface gravity of the planetesimals made melt retention difficult, and impact heating at these velocities would result in a globally averaged temperature increase of less than 50 K for a 1000 km body and less than 0.1 K for a 10 km diameter body.

The planetesimals considered by Keil et al. (1997) were non-porous objects (i.e. they contained no void space). The physical properties of planetesimals at the start of runaway growth are not known. However, recent experimental and numerical work suggests that the low velocities at which dust aggregation occurred would have resulted in the formation of highly porous (>65% pore space by volume) centimetre-scale dust aggregates (Blum, 2003; Wurm et al., 2001, 2004). Whether planetesimals formed from such aggregates via further low velocity collisions or via some form of gravitational instability (e.g., Johansen et al., 2007; Cuzzi et al., 2008), the aggregational process is expected to be gentle enough that significant porosities would remain. For example, numerical aggregation calculations by Dominik and Tielens (1997) showed that as dust aggregates collide, the collisional energy is dissipated through grain restructuring. At high velocities (>10 m s^{-1}), the collisions are disruptive rather than accretional as the aggregates fragment. At low velocities, however, the aggregates accrete and pore space is produced as the grains do not fit perfectly together. Therefore those collisions that lead to accretion of kilometre-scale planetesimals are those that produce and maintain pore space between the grains. Asteroids in the asteroid belt today show a wide range of porosities, although most are much less than 60% porous (Britt et al., 2002). It is likely, therefore, that if early planetesimals were porous much of this porosity was lost over Solar System history.

If planetesimals were porous this may have important implications for the growth and thermal evolution of planetary embryos. It is well-known that the presence of porosity can dramatically increase the amount of heating and attenuate shock energy in an impact due to the large amount of energy expended crushing out the pore space (e.g., Zel'Dovich and Raizer, 1967; Kieffer, 1971; Ahrens and Cole, 1974; Melosh, 1989; Sharp and de Carli, 2006). Although it did not change their overall conclusion, Keil et al. (1997) estimated that inclusion of porosity in their model might increase the volume of impact melt by up to a factor of 5 and increase the disruption threshold by a factor of ~3 (Love et al., 1993), thereby increasing not only the heating efficiency but also the likelihood of retaining heated material on the body. However, impact heating in porous planetesimal collisions has not been studied in detail.

The importance of heating in collisions between planetesimals will depend on many factors, among them being the frequency with which planetesimals collide with one another and the velocity of such collisions. Chambers (2006) demonstrated that during the runaway growth period of Solar System evolution the number of planetesimal collisions, N, during a given time period, Δt, in an annular zone of width w centred at an orbital distance a from the Sun, is given by:

$$N = \frac{69.4\Sigma_p r^2}{P_{orb} m_p} \frac{\pi a w \Sigma_p}{m_p} \Delta t, \quad (1)$$

where Σ_p is the surface density of the planetesimals (i.e. the total mass of planetesimals per unit area of the disk), r is the planetesimal radius, m_p is the planetesimal mass and P_{orb} is the orbital period:

$$P_{orb} = 2\pi\sqrt{\frac{a^3}{G m_{\mathrm{Sun}}}}, \quad (2)$$

where G is the gravitational constant and m_{Sun} is the mass of the Sun.

The initial mass of the solar nebula is unknown; only a minimum estimate can be derived from the current mass of the planets. The traditional Minimum Mass Solar Nebula (MMSN, e.g., Weidenschilling, 1977) assumes a surface density of ~2 g cm^{-2} in the asteroid belt. The size–frequency distribution of planetesimals prior to runaway growth is also not well constrained; however, recent dynamical simulations suggest that to explain the fossil asteroid size–frequency distribution the starting distribution must have had an excess of planetesimals 10 km diameter or larger (Weidenschilling, 2009; Morbidelli et al., 2009). If we make a conservative estimate that the planetesimals in this size range make up only 10% of the mass of the disk (i.e. $\Sigma_p = 0.2$ g cm^{-2}), then for a 0.5 AU wide disk of the MMSN centred at 2.5 AU, a swarm of 10 km planetesimals can produce ~400 collisions per year (assuming a porosity of ~50%). If we assume no porosity, there is still likely to be ~40 collisions during this same time. This will expose ~0.05 Earth masses to these sort of collisions every million years within the narrow zone considered, or nearly one Earth mass throughout the terrestrial planet region of the Solar System. For comparison, the total mass of material in the terrestrial planets is less than two Earth masses. We can therefore expect collisional evolution to have affected a significant fraction of the material found in the terrestrial planets and asteroids. Indeed, collisional evolution models by Chambers (2006) suggest that planetesimal fragmentation is a unavoidable part of the planet formation process, as most of the mass of a planet comes from the fragments created during planetesimal collisions.

Collision velocity is another important factor in planetesimal heating by impacts. Keil et al. (1997) considered the effects of impacts with a relative velocity less than about 5 km s^{-1} which is typical for the current asteroid belt; however, average collision velocities between planetesimals during runaway growth may have been significantly higher. Bottke et al. (2005) showed that during this stage of planet formation, planetesimal relative velocities would have increased rapidly to 5–10 km s^{-1}. These velocities are achieved as a few larger planetary embryos gravitationally perturb the neighbouring planetesimals, increasing their eccentricities and inclinations. Similar results were found by Kenyon and Bromley (2001), who showed how a modest-sized planetary embryo (~500 km) could "stir up" the velocities of smaller planetesimals, to such an extent that the collisions will be disruptive. In addition, Weidenschilling et al. (1998, 2001) showed that planetesimals falling into resonance with Jupiter could increase their velocities relative to the nebula gas, even reaching velocities of up to 10 km s^{-1}.

A scaling law for impact melt production has been established that relates the mass of impact melt M to the mass m_i and velocity v_i of the impactor for a given target material (e.g., Ahrens and O'Keefe, 1977; Bjorkman and Holsapple, 1987; Pierazzo et al., 1997):

$$\frac{M}{m_i} = A\left(v_i^2/E_m\right)^{3\mu/2} \quad (3)$$

where E_m is the specific internal energy required to shock melt the material from the reference temperature; A and μ are material-specific constants. For non-porous materials $\mu \approx 2/3$ so that melt volume scales with the kinetic energy of the impact. Wünnemann et al. (2008) demonstrated that this scaling law is also valid for porous materials, but in this case $\mu < 2/3$ (A and E_m also change with increasing porosity). Importantly, the scaling theory applies only to impacts on an initially cold half space; it does not apply for cases where target curvature is important or where the initial temperature of the target is higher (or lower) than the reference temperature. In addition, the scaling law does not apply for values of the so-called melt number below 30 (i.e. $v_i^2/E_m < 30$). For non-porous dunite, this implies that the scaling law is not valid for impact velocities less than 13.5 km s^{-1}. Hence, to accurately quantify the effect of impact heating in planetesimal collisions of interest here, it is necessary to numerically simulate these collisions with a shock physics code. Such modelling work has shown the localised heating potential of high-velocity collisions between large bodies (Cameron et al., 1990, 1991), but only in non-porous material.

In summary, in the first few to 10 million years of Solar System evolution, collisions between porous kilometre-scale planetesimals would have been frequent and energetic events: a large fraction of material in the terrestrial planets will have been processed in impacts at velocities up to several kilometres per second. The aim of this work is to quantify the efficiency of impact heating in such collisions. Using numerical impact models, we investigate a range of collision velocities, relative body sizes, initial temperatures and planetesimal porosities. Through this thorough numerical investigation we reexamine the importance of collisions in the thermal evolution of primitive bodies in the Solar System.

2. Method

To quantify heating in planetesimal collisions we simulated the impact of two spheres of analog planetesimal material using a hydrocode. Simulations lasted for the duration of time required for the shock wave to propagate through the planetesimals. We recorded the peak shock pressure throughout the planetesimals and used this to determine the fraction of each planetesimal that experiences a shock pressure in excess of the critical pressure for melting. This section describes the details of our modelling approach.

2.1. Critical pressure for melting

In this work, the efficiency of heating in a collision was measured by comparing the volume (and mass) of material shock heated to a certain temperature, e.g. the solidus (incipient melting) or the liquidus (complete melting). That porosity can significantly reduce the critical shock pressure for melting has been demonstrated experimentally (e.g., Bauer, 1979; Hörz and Schaal, 1981; Hörz et al., 2005). For example, Hörz et al. (2005) reported the results of a reverberation shock experiment into ~40–45% porous chondritic material. They found that at 14.5 GPa all pore space was closed; at 38.1 GPa highly vesicular melts were present at grain boundaries and were occasionally pooled into pockets of melt; at 50 GPa more grain boundary melts occurred, and more commonly formed distinct pockets and pools of melt; and at 65 GPa, 50% of the sample was molten. This shows that melting occurs at significantly lower pressures in porous material than the experimentally determined critical shock pressure for melting non-porous dunite (80–100 GPa, Reimold and Stoeffler, 1978) and the value of 106 GPa derived from the ANEOS equation of state for dunite (Benz et al., 1989; Wünnemann et al., 2008). As we demonstrate in the subsequent sections this has a significant influence on heating in planetesimal collisions.

In our simulations of planetesimal collisions, we use dunite as the solid matrix component of the planetesimals. Dunite, the olivine-rich end member of peridotite, is a reasonable approximation of the chemical composition of the rocky material found in bodies in the inner Solar System. It is also a material with a relatively well-defined equation of state (derived using the analytical equation of state, ANEOS, Thompson and Lauson (1972); Benz et al. (1989)). Wünnemann et al. (2008) outline the procedure for calculating the critical shock pressure required to melt a porous material assuming that the non-porous material equation of state is known, which we describe in Appendix A. Using this method we determined the shock pressure (and entropy) for incipient and complete melting of dunite by calculating the minimum shock pressure that resulted in a post-shock temperature above the solidus and liquidus temperatures. We defined the dunite melting curves using data for peridotite (McKenzie and Bickle, 1988; Katz et al., 2003). The entropy for incipient and complete melting of dunite were 2785 and 3270 J kg^{-1} K^{-1}, respectively. These values of entropy apply for all initial porosities and for an initial temperature of 298 K. They are lower than the values previously defined by Pierazzo et al. (1997), which correspond to a higher dunite melt temperature, appropriate for pure forsterite. Fig. 1 plots the critical shock pressure for incipient melting of dunite, P_{sol}, as a function of porosity ϕ. It shows the significant effect that porosity has on the critical pressure for melting. For non-porous bodies, P_{sol} = 102 GPa and P_{liq} = 128 GPa. At 12% porosity, P_{sol} is approximately half of that value (51.6 GPa), at 30% porosity, P_{sol} = 18.7 GPa, and at 50% porosity P_{sol} = 7.87 GPa. This will clearly have a significant effect on the volume of material shock heated to the melting point as porosity increases.

Fig. 2 shows the effect of initial temperature on the critical pressure for incipient (solidus) and complete (liquidus) melting (P_{sol} and P_{liq}, respectively). As the initial temperature of the material is increased, so the pressure needed to shock heat it to the solidus or liquidus decreases. For low porosity material, $P_{liq} \approx 26$ GPa higher than P_{sol} (for an initial temperature of 298 K). Intuitively, the hotter material is prior to shock, the easier it is for the material to be shock heated to T_{sol}, which has been shown experimentally by Huffman and Reimold (1996). Schmitt (2000) also found that shock experiments which start at a higher temperature produce a larger volume of melted material, and the onset of shock melting occurs at lower shock pressures.

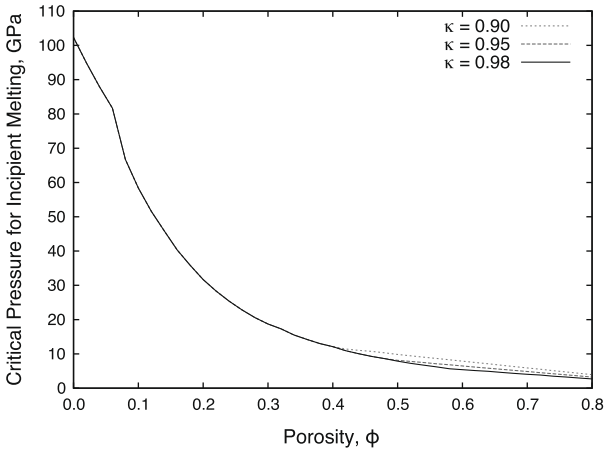

Fig. 1. As porosity increases, the critical pressure for incipient melting (the pressure needed to shock heat the material to the solidus in a single shock wave) decreases. This is well defined for $\phi < 50\%$, and above 50% is dependant on the compaction rate parameter chosen (κ) in the porous-compaction model (see text for details).

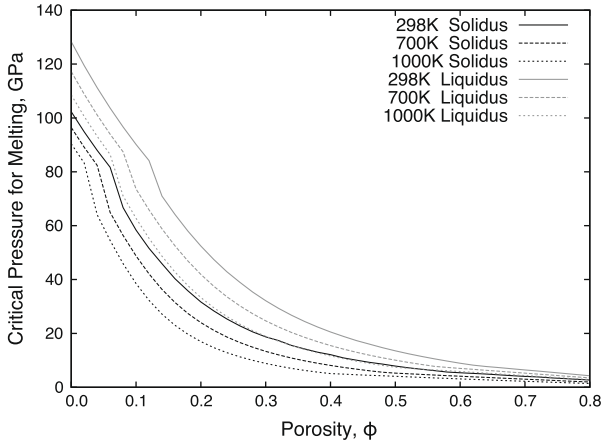

Fig. 2. The effect of porosity on the critical pressure for incipient and complete melting. Warmer bodies require a lower shock pressure to induce melting.

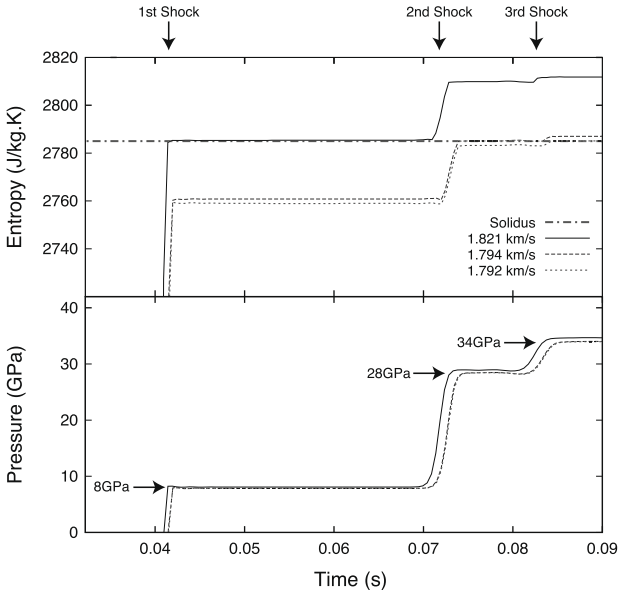

Fig. 3. The increase in entropy and pressure through time in simulations of an iron flyer plate impacting into a 50% porous dunite sample. Three distinct increases in shock pressure and entropy can be seen as the shock wave first passes through the material (first shock), then reflects from a buffer plate (second shock) and then once again from the impacting plate (third shock). Shown are the results for three different impact velocities. At 1.821 km s^{-1}, the dunite is shock heated to the solidus in the first shock wave (the critical shock pressure required for melting in this case is ~8 GPa). At 1.794 km s^{-1}, after the first reflection of the shock wave the entropy of the material is above the critical entropy required to melt the material (~28 GPa), and at 1.792 km s^{-1}, a second reflection was required to melt the material (~34 GPa).

As discussed above, Hörz et al. (2005) estimated the shock pressure required to melt a chondritic powder of 40–45% porosity, based on shock reverberation experiments. In an experiment that achieved a peak shock pressure of 14.5 GPa, no melt was observed, but in an experiment that achieved a peak shock pressure of 38.1 GPa, melt was observed at the grain boundaries. Unlike our calculations of the critical shock pressure for melting, which assume loading occurs in a single shock, loading in reverberation experiments is achieved in multiple stages, first via the initial impact-induced shock wave, then by subsequent reflected shock waves from the back of the sample and the interface between the sample and impactor. The shock reverberation technique requires less *PdV* work to reach the maximum shock pressure, and hence produces less waste heat during unloading, for a given overall shock pressure. These experiments therefore overestimate the critical pressure required for melting in a single shock wave.

To compare our calculations of the critical pressure for melting with experimental results we simulated planar impacts analogous to those experiments of Hörz et al. (2005) using a hydrocode (see Section 2.3). We simulated the impact of an iron plate into a sample of porous dunite buffered by another iron plate, at various velocities. The shock pressure and entropy in the dunite sample were recorded after the incident shock wave, after the first reflection from the buffer plate and after the second reflection from the impacting plate. Results are presented in Fig. 3. For a 50% porous dunite target, at an impact velocity of 1.821 km s^{-1} the entropy required for melting was reached in a single shock—in this case the peak shock pressure was ≈8.1 GPa, which is consistent with our calculations above (see Fig. 1). At an impact velocity of 1.794 km s^{-1} the material was shock heated to the solidus in two stages (i.e. the initial shock wave and its reflection)—in this case $P_{sol} \approx 28.4$ GPa, more than a factor of three higher than that required in a single shock. For an impact velocity of 1.792 km s^{-1}, three stages were required to reach the entropy required for melting (i.e. two reflections of the shock wave), and $P_{sol} \approx 34.0$ GPa. Similar results were observed for a 40% porous target. These simulations demonstrate that the critical pressure required to shock heat a material to the solidus in one shock wave can be substantially smaller than that required in a multi-shock, reverberation experiment. Moreover, the high impedance contrast between the porous dunite sample and the iron flyer and buffer plates, combined with the fact that pore space is fully compacted after the first shock, mean that the second shock can be stronger (i.e. a larger increase in pressure across the shock) than the first shock. Our simulations of shock loading in two/three stages predict a critical pressure for melting 40–50% porous dunite of ~28–35 GPa, which is consistent with estimates of the critical pressure for melting a ~45% porosity chondritic powder based on reverberation shock experiments by Hörz et al. (2005), and reiterate that shock melting in one shock stage can be achieved at even lower shock pressures.

2.2. Limitations

Wünnemann et al. (2008) discuss the limitations of the above approach for quantifying the thermodynamic state of a porous material, which are inherent to the porous-compaction model and the dunite ANEOS equation of state. The limitations of ANEOS for deriving equations of state for geologic materials are discussed by Ivanov (2005) and Melosh (2007). An important limitation of the ANEOS-derived dunite equation of state used in this work is that it does not include latent heat of melting. Consequently, the equation of state over-estimates temperatures in excess of the melt temperature and the critical shock pressure for melting is slightly under-estimated. To provide a measure of uncertainty in our calculations we also compute the critical pressure for complete melting (i.e. the pressure required to raise the temperature above the liquidus on release, P_{liq}). The actual critical pressure for incipient melting will be bounded between these limits, but is likely to be closer to the lower-bound estimate.

A shortcoming of the compaction model is that the compaction function for planetesimal-analog materials are not well constrained. Ideally, the compaction function would be determined empirically using crush data for planetesimal-analog materials of varying porosities. In the absence of this data, we used representative values for the compaction parameters that have provided good fits to other porous geologic materials and explored the sensitivity of our results to these parameters. The critical pressure for melting dunite (Fig. 2) is unaffected by the compaction rate parameter (κ, see Appendix A) used in the porous-compaction model for porosity

values from 0% up to approximately 40–50%. This is because, for low porosities, the pore space is compacted out of the material at a shock pressure lower than P_{sol}. For higher porosities, the assumed compaction rate affects the critical pressure. A value of κ very close to 1 is most realistic for highly porous materials as very little compression of the matrix occurs before all pore space has been compacted. Moreover, for some materials the solid matrix material may actually expand during compaction due to the extreme heating involved (Zel'Dovich and Raizer, 1967). This would imply a κ-value greater than one for a portion of compaction. For lower values of κ, we find that P_{sol} is higher in very porous material ($\gtrsim$ 50% porosity). Fig. 1 presents several values of κ for comparison. For example, at 60% porosity, P_{sol} = 7.89 GPa for κ = 0.90, but P_{sol} is only 5.40 GPa for κ = 0.98. A value of κ = 0.98 has previously been found to be a good fit to Hugoniot data for a range of moderately porous materials (Wünnemann et al., 2006, 2008), and is used for the results presented in this study.

The compaction model is a continuum approximation of the macroscopic behaviour of a porous material. As such, it assumes that pore sizes are below the resolution of the model, which in our simulations is ~1/500 times the radius of the planetesimal (~10 m cell size), and that pores are uniformly distributed within the material. As long as this assumption is valid, the results presented here should be independent on the exact scale and nature of the pore space. The model implicitly assumes that shockwave compaction and heating are homogeneous within the material; hence, the critical pressure for melting calculated here and any heating induced by pore collapse represent averages over the bulk material. In natural materials, pore spaces occur on a wide range of scales and are often non-uniformly distributed; hence, their compaction can be quite heterogeneous and lead to highly-localised heating "hotspots" (e.g. Kieffer et al., 1976) on the scale of single pores.

2.3. Initial conditions for the model

To simulate planetesimal collisions we use the iSALE hydrocode (Collins et al., 2004; Wünnemann et al., 2006), which is an extension of the SALE hydrocode (Amsden et al., 1980) and is similar to the SALEB hydrocode (Ivanov et al., 1997; Ivanov and Artemieva, 2002; Ivanov, 2005). To simulate hypervelocity impact processes in solid materials SALE was modified to include an elasto-plastic constitutive model, fragmentation models, various equations of state (EoS), and multiple materials (Melosh et al., 1992; Ivanov et al., 1997). More recent improvements include a modified strength model (Collins et al., 2004) and a novel porosity compaction model (Wünnemann et al., 2006). The code is well tested against laboratory experiments at low and high strain-rates (Wünnemann et al., 2006) and other hydrocodes (Pierazzo et al., 2008). Wünnemann et al. (2008) used iSALE to quantify the effect of porosity on melt production in sedimentary rocks.

iSALE is a two-dimensional hydrocode that employs axial symmetry. This limits impact events to normal incidence angles, and collisional events to a head-on, direct impact geometry. The duration of each simulation was just long enough to follow the generation, propagation and release of the shock wave in each collision. In this phase of cratering the effects of material strength and gravity are negligible; hence, both strength and gravity were omitted from our calculations.

The majority of simulations were of two 10 km diameter bodies colliding, apart from simulations investigating the effect of relative body size. A diameter of 10 km was chosen as being typical of planetesimals during the runaway and oligarchic growth phases of the evolution of the Solar System. However, as our model does not include gravity or strength, our results are independent of planetesimal size (provided the assumption that pore spaces are small compared to the finest mesh size still holds) and we present our results in dimensionless units. The temperature profile of the solar nebula is not well understood, and would likely have changed significantly through time. We therefore used the reference temperature from the dunite equation of state, 298 K, as the initial planetesimal temperature. This is well within the temperature range suggested by previous studies (e.g., Cassen, 1994), and later investigated the effect of changing this parameter.

Planetesimal porosity was varied between 0% (non-porous) and 80%. At extreme porosity ($\gtrsim$ 70%), the compaction function in the ϵ-α porous-compaction model is inaccurate (Wünnemann et al., 2008) as it does not allow for matrix expansion during compression (e.g., Zel'Dovich and Raizer, 1967; Jutzi et al., 2008). However, such high porosities are unlikely to have been typical of planetesimals. As discussed above, the compaction rate, κ, has little effect on shock heating for <50% porosity. Impact velocity was varied between 1 and 20 km s^{-1} to span the complete range of collision velocities suggested by studies of planetesimal stirring during runaway growth (Weidenschilling et al., 1998, 2001; Kenyon and Bromley, 2001; Bottke et al., 2005; Chambers, 2006).

2.4. Measuring the mass of shock heated material

The method for determining the mass of material that experiences a peak shock pressure greater than a certain threshold pressure is discussed in Pierazzo et al. (1997), Pierazzo and Melosh (2000) and Ivanov and Artemieva (2002). To track the pressure-history of material in a calculation, iSALE uses 'mass-less' (Lagrangian) tracer particles. These particles are assigned at the beginning of the simulation to a certain mass of material (typically, that contained within one computational cell), and follow the path of this mass through the course of the collision event. The total mass of material that experienced a certain threshold pressure or greater is the sum of the mass of all the tracer particles in the mesh that experienced a maximum shock pressure in excess of this threshold pressure. By defining the threshold pressure as the calculated critical pressure for melting, for example, it is possible to then compare how efficient each collisional event is at melting the planetesimal material.

2.5. Resolution

In iSALE, a discrete grid of cells is used to represent the region in which the collision occurs. The smaller the size of these cells, the more accurately the propagation of a shock wave can be resolved. However, this increase in resolution comes at the cost of computational time, so a suitable balance must be found. The convention in impact modelling is to measure the resolution of a simulation in terms of the number of cells per projectile radius, CPPR. To test the dependence of heating on CPPR, several series of simulations of equal-sized porous dunite bodies were run, in each series keeping the initial conditions (porosity, velocity, initial temperature) constant, changing only the resolution. By increasing the resolution, the measured mass of material shock heated to a certain temperature (e.g. $M(>T_{sol})$, where T_{sol} is the solidus temperature) increases. Following the method suggested by Boris Ivanov (personal communication) this can be approximated by an exponential function of the inverse of the resolution (1/CPPR), which gives the 'true' value of $M(>T_{sol})$ when 1/CPPR = 0 (i.e. at hypothetical 'infinite' resolution). By normalising $M(>T_{sol})$ by this 'true' value (Fig. 4), it is easy to see by how much the model underestimates the mass of shock heated material due to the resolution. Fig. 4 shows that the amount that the model underestimates the shock heated mass depends not only on 1/CPPR, but also on the efficiency of heating in the collision. In a previous calculation for impacts at 18 km s^{-1} into a porous half space target using the iSALE hydrocode,

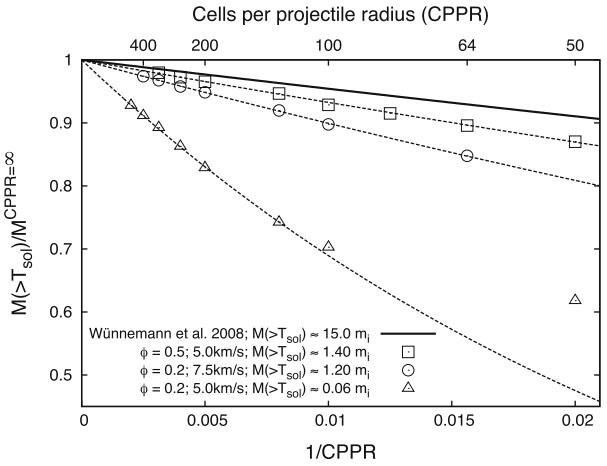

Fig. 4. Resolution study of several different planetesimal collision set ups. As less mass is shock heated to the solidus (relative to the impactor mass), the need for higher resolution increases. For comparison, the resolution study of impacts into a half space from Wünnemann et al. (2008) is shown.

Wünnemann et al. (2008) found that a resolution of 80 CPPR was required to limit the error to just 5% (note that this is only the error induced in the model due to the resolution used). In that case, $M(>T_{sol}) \sim 15m_i$, where m_i is the impactor mass. For two 50% porous dunite planetesimals colliding at 5 km s^{-1}, a much smaller mass of material is shock heated to T_{sol} ($M(>T_{sol}) \sim 1.4m_i$), so a greater resolution of 150 CPPR is required to produce an error of 5%. For 20% porous planetesimals colliding at the same velocity, a resolution of 650 CPPR is required to produce an error of 5%, when $M(>T_{sol}) \sim 0.06m_i$. A resolution greater than that employed in previous impact studies using iSALE (e.g., Wünnemann et al., 2008) is therefore required for simulations of colliding planetesimals at velocities of ~5 km s^{-1}, due to the lower ratio of shock heated mass to impactor mass. Throughout this study, we use a resolution of ~500 CPPR, and the errors induced by this resolution underestimate the amount of heated material by ~1–10%. A similar accuracy may be achieved with a lower resolution by using a higher-order accuracy computation scheme (e.g. CTH; see, Pierazzo et al., 1997).

3. Results

3.1. A collision event

Fig. 5 shows results from two models of two equal-sized dimensionless bodies colliding at a relative collision velocity of 5 km s^{-1}. The initial temperature of the bodies in this case is 298 K. The left images depict the results of two non-porous planetesimals colliding; the right images depict the results of two 50% porous planetesimals. There are several important stages to note. During the initial contact stage, a shock wave travels through both bodies from the point of contact towards the back edge of the bodies. In non-porous bodies, a very high shock pressure can be reached (>100 GPa). In porous bodies, the shock energy is attenuated by the crushing of pore space. As a result, the shock speed is substantially reduced (e.g. it takes twice as long for 50% of the material to experience the shock wave) and lower shock pressures are reached (<25 GPa). The high pressure zone is confined to a much more localised region when compared to the non-porous case (for example, only one-hundredth of the mass is shock heated above 20 GPa in the non-porous collision, compared to a third of the mass shock heated to the same pressure in the porous collision). Fig. 5A highlights these differences, showing the pressure in the planetesimals 1 s after impact—note that in the non-porous case the shockwave

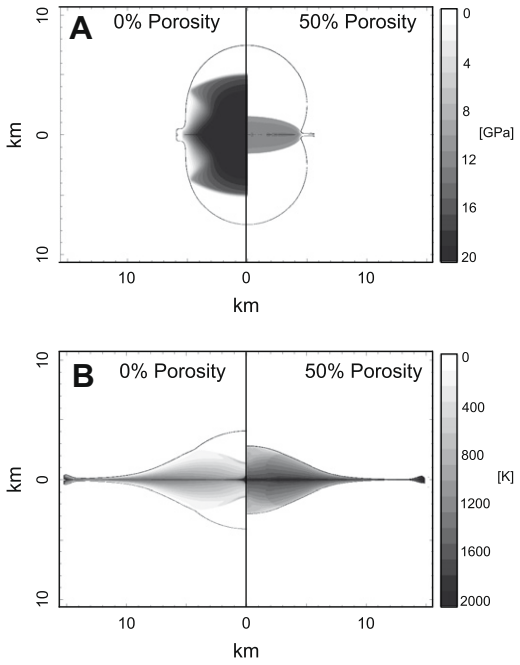

Fig. 5. (A) Comparison in the early stages of the model showing the difference in pressures between porous and non-porous bodies. Non-porous material experiences much higher shock pressure, because no work is needed to close pore spaces. Attenuation of the shock front is greater in porous material. (B) Comparison of the final temperature profiles of the same two simulations (at a later time step to A, after the release from high shock pressure). The non-porous case shows only localised heating through the centre of the resulting body of material. The volume is much lower in the porous case, as much of the pore space has been crushed out. However, most of this volume is still at significantly high temperatures (e.g. >1000 K), whereas in the non-porous case much of the material (from the back edge of the colliding bodies) has experienced little to no temperature rise. This extra increase in temperature is due to the extra waste heat produced in porous materials (see text for details).

has travelled further into the planetesimal and generated far higher pressures behind the shock front than in the porous case.

The next important stage in the collision process is the propagation of a release wave. This is initiated at the point in time when the shock wave reaches the edge of one or both of the bodies (a free surface). In the idealised cases considered here where both bodies are identical in volume and porosity, this will be at the same time. The release wave acts to decompress the material from the high shock pressures, and allows materials to reach their shock-heated temperatures. In the models shown in Fig. 5 the temperatures experienced by the colliding bodies during the course of the simulation are also recorded. Fig. 5B shows the final temperature profiles of the two models. After the release from high shock pressure, almost all the material in the porous collision has been heated, with the majority of material above 1000 K. In the non-porous simulation, only a thin band of material has reached this temperature. The material from the back of the planetesimals in the non-porous case has not experienced a significant temperature increase compared to the material from the back of the porous planetesimals, despite experiencing higher shock pressures. This is a result of the lower waste heat generated in non-porous planetesimal collisions.

Note also that at this stage of the collision process a high velocity jet of material is expanding radially away from the contact site in the plane perpendicular to the collision velocity. Material in this jet is very low density, and is still accelerating at the end of the simulation.

Over 300 simulations similar to the two depicted in Fig. 5 were performed in a comprehensive quantitative study of disruptive

collisions between planetesimal bodies. The following sections describe the effects that porosity, velocity, relative body size and initial body temperature have upon heating in planetesimal collisions.

3.2. The effect of porosity

Table 1 and Fig. 6 present results of collisions between two equal-sized dimensionless, spherical, dunite planetesimal bodies, for a range in porosity from 0% up to 75%. We start here with a relative collisional velocity of 5 km s^{-1} (see Section 3.3 for a discussion of the effect of the collision velocity). In non-porous and low porosity bodies, there is very little material shock heated to the melting point (at this velocity), which agrees with the results presented in Keil et al. (1997). As the pore space volume is increased up to ~50%, the fraction of the planetesimal for which $T > T_{sol}$ after release (i.e. the shock heated mass normalised by the total initial mass of the planetesimals $M(>T_{sol})/(m_i + m_t)$) increases considerably, and can be fit by a power law (Fig. 6). For very porous bodies ($\gtrsim$ 50% porosity), the mass of shock heated material depends upon the porous compaction parameter κ, decreasing as κ decreases. This is due, in part, to the increase in P_{sol} for lower κ. The compaction rate also affects the attenuation of the shock wave. As mentioned above, a value of 0.98 seems to fit Hugoniot data well; also presented are results for $\kappa = 0.95$ and $\kappa = 0.90$ to illustrate the sensitivity of these results on κ.

Table 1 and Fig. 7 also detail the change in the *absolute* mass of material for which $T > T_{sol}$ after release in these collisions (i.e. the shock heated mass normalised by the mass of two non-porous planetesimals $M(>T_{sol})/(m_i + m_t)^{\phi=0}$). By normalising by a constant amount, a slightly different trend is apparent. There are two competing controls on the absolute mass of material shock heated to T_{sol} as porosity increases. Acting to reduce the absolute mass of shock heated material is the increasing proportion of pore space (a porous material has a lower mass for a given volume). The shock heated mass increases, however, due to the second control—the lower critical pressure for melting at higher porosity. For porosities up to approximately 50%, a power law relationship still exists (Fig. 7). This power law relationship for the mass heated to the solidus breaks down for porosities higher than ~45%. In even more porous material (above ~60% porosity), the lower initial mass is the dominant factor, and a reduction in the absolute mass of material shock heated above T_{sol} is observed. The porosity at which the power law no longer fits the data for the liquidus is higher than that seen for the solidus (in this case it is for >60% porosity), and a decrease in the absolute mass of material shock heated to the liquidus occurs for porosities greater than 70%.

Table 1
Simulation results for two dimensionless dunite spheres colliding at 5 km s^{-1}. $M(>T_{sol})/(m_i + m_t)^{\phi=0}$ is the mass of material shock heated to the solidus, normalised to the initial mass of the two planetesimals in the non-porous simulation, and $M(>T_{sol})/(m_i + m_t)$ is the fractional mass of material shock heated to the solidus relative to the total initial mass of the two colliding bodies. $\kappa = 0.98$.

Porosity (%)	Initial mass	$\frac{M(>T_{sol})}{(m_i+m_t)^{\phi=0}}$	$\frac{M(>T_{sol})}{(m_i+m_t)}$
0	1.00	0.000	0.000
10	0.90	0.000	0.000
15	0.85	0.010	0.011
20	0.80	0.025	0.031
25	0.75	0.050	0.067
29	0.71	0.075	0.105
33	0.67	0.115	0.173
38	0.63	0.168	0.269
40	0.60	0.203	0.340
45	0.55	0.266	0.485
50	0.50	0.320	0.640
55	0.45	0.351	0.779
60	0.40	0.345	0.862
68	0.32	0.282	0.883
75	0.25	0.224	0.894

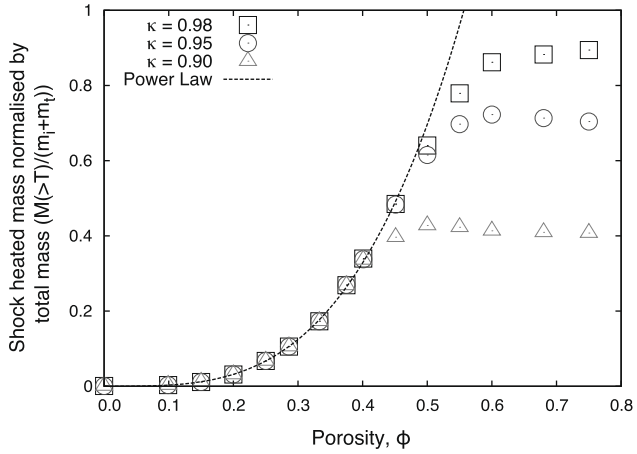

Fig. 6. Non-porous materials experienced very little material being shock heated above the solidus. As porosity increases, we see a significant increase in the proportion of the initial mass which is shock heated above the solidus (fit by a power law curve) up to ~50%. The proportion of the initial mass that is shock heated to the solidus levels off in highly porous material. For comparison, several values of κ are presented, showing the effect of compaction rate in highly porous material. Results are for collisions between two equal-sized, dimensionless bodies at 5 km s^{-1}.

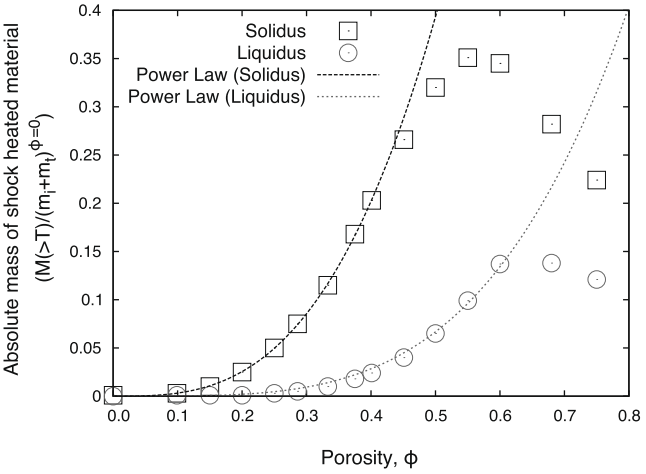

Fig. 7. As porosity increases, the mass of material which is shock heated above the critical pressure for melting increases by a power law function to ~40–50% porosity, above which we see a reduction in the mass of material melted due to the decrease in initial mass (as the material has a higher pore fraction). Results are for collisions between two equal-sized, dimensionless bodies at 5 km s^{-1}, and are normalised to the mass of two non-porous bodies, $(m_i + m_t)^{\phi=0}$.

3.3. The effect of collision velocity

As the kinetic energy involved in a collision increases, the shock pressures will increase and hence the amount and extent of heating will increase. Fig. 8 and Table 2 show the effect of collision velocity on melt production for the case of equal-sized planetesimals for different planetesimal porosities (non-porous, 20% porosity and 50% porosity).

For non-porous planetesimals a very high velocity is required to shock heat the total mass of both bodies to T_{sol} (and T_{liq}); heating in collisions at several km s^{-1} is small. For example, in non-porous bodies colliding at ~5 km s^{-1}, a negligible mass is shock heated to T_{sol}. However, at velocities above ~15 km s^{-1}, it is possible to

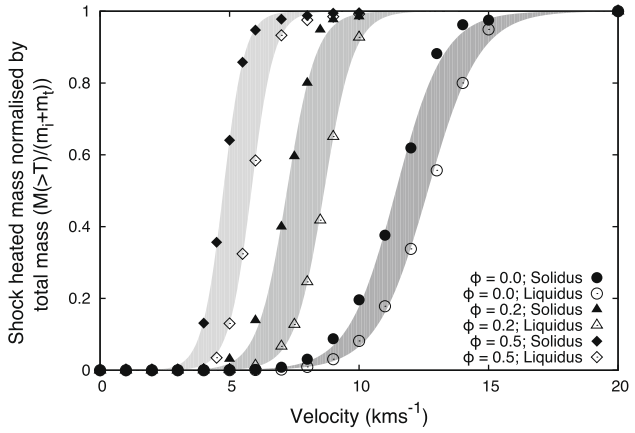

Fig. 8. The effect of velocity on the mass of material shock heated to the solidus. Two important effects are shown—increasing velocity results in a higher fraction of the original material mass being shock heated to the solidus, and an equivalent mass of shock heated material can be produced at lower velocities in higher porosity material. Results are for collisions between two equal-sized, dimensionless bodies, and are normalised to the total mass of material ($m_i + m_t$).

Table 2
Results for non-porous, 20% and 50% porous bodies colliding at a range of velocities. Presented here is the fraction of the initial mass shock heated to the solidus ($M(>T_{sol})/(m_i + m_t)$).

Velocity (km s^{-1})	$\frac{M(>T_{sol})}{(m_i+m_t)}$		
	$\phi = 0$	$\phi = 0.2$	$\phi = 0.5$
3	0.000	0.000	0.000
4	0.000	0.003	0.131
5	0.000	0.031	0.641
6	0.000	0.139	0.947
7	0.008	0.400	0.978
8	0.031	0.800	0.988
9	0.088	0.977	0.995
10	0.196	0.985	0.996
11	0.376		
12	0.619		
13	0.882		
14	0.962		
15	0.975		

shock heat almost the whole body to T_{sol} (when >0.97 ($m_i + m_t$) is shock heated to at least T_{sol}). To shock heat 0.50($m_i + m_t$) to T_{sol}, a velocity of ~11.5 km s^{-1} is required; to shock heat ~ 0.05($m_i + m_t$) to T_{sol} a velocity of ~8.5 km s^{-1} is required.

When the colliding bodies are increasingly porous, the fraction of material shock heated to T_{sol} increases. Therefore, a lower velocity is required to achieve the same level of shock heated material when the porosity is higher. For example, for two colliding 20% porosity dunite bodies, a velocity of ~7.2 km s^{-1} will shock heat 0.50($m_i + m_t$) to T_{sol}, and in 50% porosity dunite, ~4.8 km s^{-1} is sufficient to reach this fraction of shock heated material. This is due to the lower P_{sol} in more porous material. An increase of relative velocity by approximately 1–1.5 km s^{-1}is sufficient to shock heat an equivalent mass of material to T_{liq}.

Even if the collision velocity is too low to produce much melt, shock heating may still be significant. For example, in an impact between two planetesimals with 50% porosity at 3 km s^{-1} almost the entire planetesimal mass is heated by >400 K and ~40% is heated by >700 K.

3.4. The effect of initial temperature

During impact, planetesimal material is melted by raising its internal energy through the conversion of kinetic energy. Hence, if the planetesimal's initial internal energy is higher, less kinetic energy is required to induce melting. This can be achieved by increasing the initial temperature of the planetesimals (for example by radioactive heating by ^{26}Al decay or even by heating from previous impacts). Fig. 9 shows the effect of porosity on melt production in equal-body collisions at 5 km s^{-1} for different initial temperatures (298 K, 700 K and 1000 K). Significant impact heating of lower porosity material can be achieved if the initial temperature is higher. For example, the same relative mass of material shock heated to the solidus is achieved if the planetesimals have an initial porosity of 45% and an initial temperature of 298 K or if the initial porosity is 25% and the initial temperature is 1000 K.

3.5. The effect of relative body size

Collisions between objects of the same size will be relatively rare in the Solar System, compared to those between bodies of differing size. Hence, we varied the relative size of the two colliding bodies from a impactor-to-target planetesimal mass ratio (m_i/m_t) of 1:1 down to a mass ratio of 1:1000. To quantitatively compare the results between simulations, the total volume of the two colliding bodies was kept equal. Simulations of 5 km s^{-1} collisions were performed for porosities between 20% and 50%. The results are presented in Figs. 10 and 11.

Fig. 10 shows the mass of material shock heated to various temperatures (including the solidus) normalised by the smaller planetesimal mass ($M(>T)/m_i$) in the collision as a function of relative body size (m_i/m_t), for 50% porous dunite. It shows that, below an impactor-to-target planetesimal mass ratio of 0.1 and for a collision velocity of 5 km s^{-1} the mass of material shock heated to above the solidus is ~2 times the smaller planetesimal mass, and the mass shock heated by 100 K is ~9 times the smaller planetesimal mass. When the bodies are of approximately equal size these values drop to about 1.5 and 2, respectively. At a collision velocity of 10 km s^{-1} about 3–4 times more material is heated to a given temperature. In cases where the impactor is small compared to the target body, traditional scaling laws may be applied (as the collision geometry more closely resembles an impact into a half space and the point source approximation). Our results show a slight reduction in mass shock heated to a given temperature with reducing planetesimal mass ratio below $m_i/m_t \sim 0.1$. This is an artefact due to the lower resolution used in simulations with a low impactor-to-target mass ratio. In reality, for small impactor-to-target

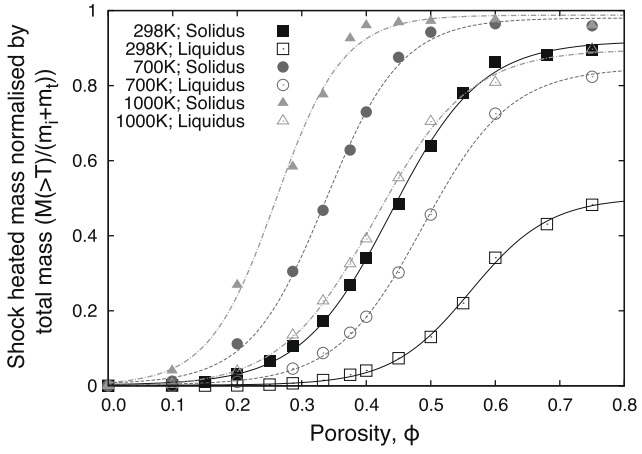

Fig. 9. Results for collisions between two equal-sized, dimensionless planetesimals colliding at 5 km s^{-1}, for bodies with initial temperatures of 298 K, 700 K and 1000 K. Shock heated masses are normalised by the total mass of material ($m_i + m_t$).

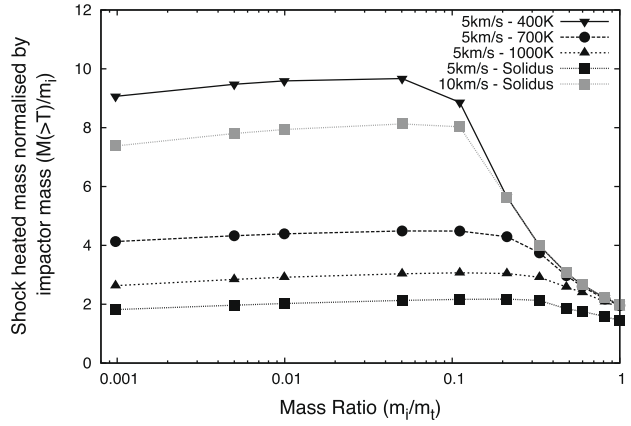

Fig. 10. The effect of impactor-to-target planetesimal mass ratio (m_i/m_t) on the efficiency of heating for 50% porous dunite planetesimals with an initial temperature of 298 K, colliding at 5 and 10 km s^{-1}. Shock heated masses are normalised by the impactor mass, m_i. For a mass ratio of 0.1 or less, ~9 times the impactor mass is heated by 100 K; ~4 times the impactor mass is heated by 400 K, and ~3 times the impactor mass is heated by 700 K. ~2 times the impactor mass is heated to the solidus in a 5 km s^{-1} collision, compared to ~8 times the impactor mass in a 10 km s^{-1} collision.

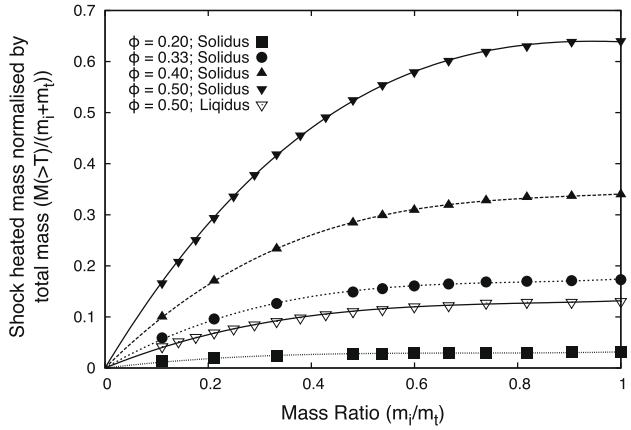

Fig. 11. The effect of impactor-to-target planetesimal mass ratio (m_i/m_t) on the efficiency of heating for two 50% porous planetesimals colliding at 5 km s^{-1}. Results shown here are as a fraction of the total mass of material ($m_i + m_t$). The most efficient heating is when the bodies are of equal size.

mass ratios the mass shock heated to a given temperature will be a constant multiple of the impactor mass.

The proportion of the impactor that is shock heated to the solidus is unchanged for all mass ratios (approximately 75% of the impactor at 5 km s^{-1} and almost the entire impactor at 10 km s^{-1}). For mass ratios below ~0.1, approximately 35% of all material shock heated to the solidus comes from the impacting body at 5 km s^{-1} and this value falls to ~12% for collisions at 10 km s^{-1}. For both 5 km s^{-1} and 10 km s^{-1} collisions, only approximately 10–15% of the mass shock heated by 100 K comes from the impactor for planetesimal mass ratios below 0.1.

If the data is normalised to the total initial mass, rather than the mass of the impactor, then it is evident that the most efficient collision for heating the largest total mass of material is when the colliding bodies are of equal size. This is shown in Fig. 11, which plots the proportion of the total planetesimal mass shock heated above the solidus $M(>T_{sol})/(m_i + m_t)$ versus relative body size. As the mass ratio decreases, $M(>T_{sol})/(m_i + m_t)$ decreases. However, it is important that even in the case of a planetesimal mass ratio of 1:10, more than 5–15% of the total planetesimal mass is heated to the solidus if the planetesimals have moderate porosity (30–50%) and a relative velocity in excess of 5 km s^{-1}. In the case of similar sized planetesimals (with a mass ratio of ~1:1), the collision will be disruptive. However, it is also these collisions which produced the largest fraction of heated material in a single shock event.

When two equal size bodies collide, the shock front travels through both bodies symmetrically, until it reaches the far edge of both bodies simultaneously (see Fig. 12B). At this point the release wave travels from the outer edge of the bodies, towards the centre of the colliding bodies (Fig. 12C). Because the shock wave is able to propagate far into both bodies, most of the material experiences shock pressures that, especially in more porous material, produce substantial heating and melting after release (see Fig. 12).

In bodies of unequal size, once the shock wave has reached the back edge of the smaller body, (Fig. 13B) the release wave moves back through first the small body, and then the larger body (Fig. 13C), before catching up to the shock front in the large body. This prevents the area towards the back edge of the large body reaching high shock pressures (and therefore high temperatures after release). As the colliding bodies become more different in size, this effect becomes more important, as the release begins earlier with respect to the time it takes the shock wave to propagate through the larger body.

4. Discussion

Our investigations have quantified the effects of four variables on heating during planetesimal collisions: the relative collision velocity, the initial porosity and temperature of the planetesimal material and the relative size of the planetesimals. We have shown that collisions between planetesimals at several kilometres per second can cause significant heating and melting if, as expected, planetesimals are highly porous. For initially cold planetesimals with a porosity of ~50%, a collision velocity of 5 km s^{-1} is sufficient to melt a total mass on the order of the 1–2 times the mass of the smaller of the two bodies. Such collisions also heat a mass approximately 4 times the mass of the smaller body to ~700 K, which could result in low temperature alteration as observed in many meteorites; and 9–10 times the impacting mass may be heated by >100 K, which could be important for vaporising water, for example. In contrast, and consistent with previous modelling studies of heating in small-body collisions (Love and Ahrens, 1996; Keil et al., 1997), if the planetesimals have no porosity heating is negligible for collision velocities less than ~7 km s^{-1} and small for velocities less than 10 km s^{-1}.

The extent of heating increases substantially for higher collision velocities and the potential for melting increases if the initial temperature of the planetesimal material is higher. For example, in collisions between equal-sized, 50% porous planetesimals, at an initial temperature of about 300 K and at an impact velocity of 5 km s^{-1} about one half of the *total* mass of both planetesimals is heated above the solidus; whereas, complete melting of both bodies occurs at an impact velocity of 7 km s^{-1} or if the initial temperature is 700 K. Impact velocities up to 10 km s^{-1} and internal planetesimal temperatures up to 1000 K were possible in the first few million years of embryo growth. Such high temperatures may be achieved from the decay of short-lived radio-nuclides.

A complete assessment of the importance of collisional heating in Solar System evolution is beyond the scope of this study. This requires knowledge of the frequency of collisions between planetesimals as well as the relative body sizes, the collision velocity and the change in planetesimal porosity with time as small impacts compact out porosity in larger bodies. However, the results of our numerical simulations can be used to derive a first-order estimate of the extent of impact heating on a porous planetesimal. To

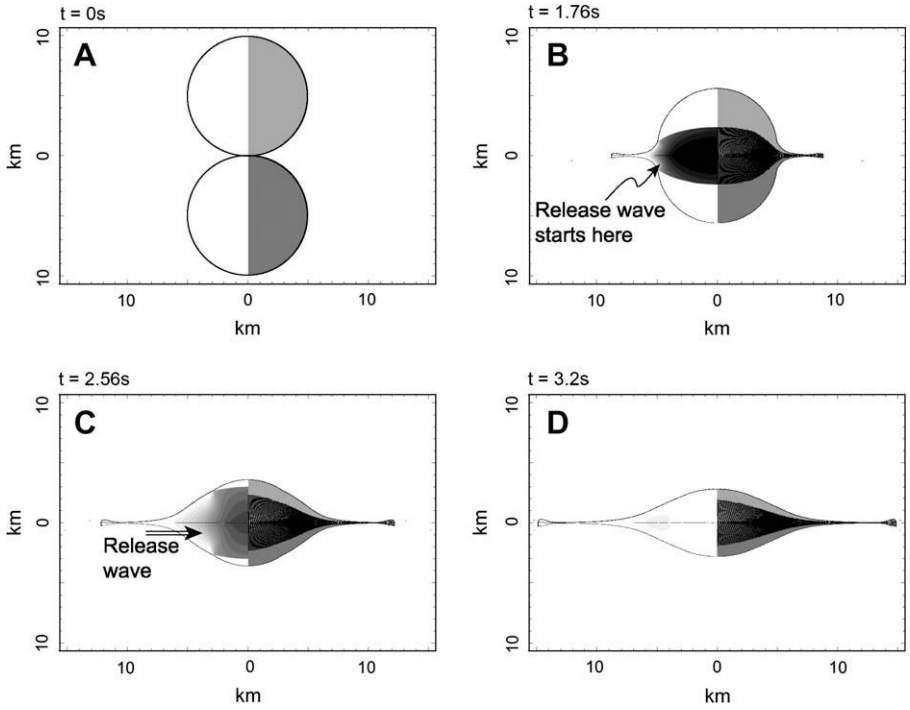

Fig. 12. Selected timesteps for two equal volume bodies (starting diameter 10 km), colliding at 5 km s^{-1}. The initial porosity is 50%. The left hand side of each plot displays the pressure (white is low pressure, black is high pressure). On the right hand side, the black particles represent those tracer particles that have been shock heated above the critical pressure for melting (~8 GPa). (A) shows the initial model setup. (B) is at t = 1.76 s, and shows the shock wave reaching the outer edge of the body, just before the release wave propagates inwards. (C) shows the release wave mid-way through the bodies, and (D) is after the shock pressure has been fully released.

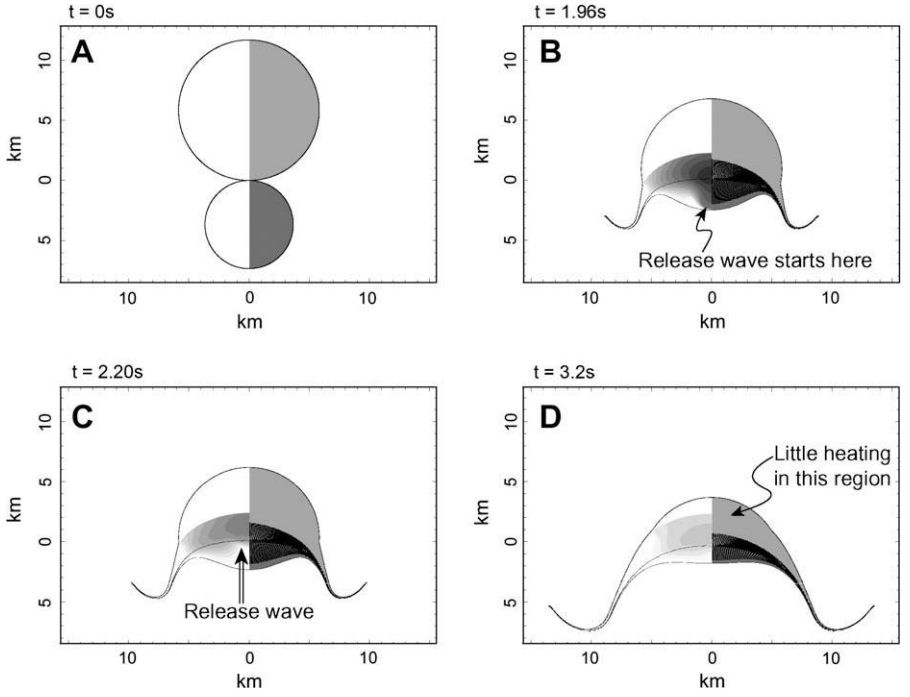

Fig. 13. Selected timesteps for two 50% porosity bodies colliding at 5 km s^{-1}. In this simulation the two initial bodies have different volumes (the larger body has a volume four times greater than the smaller body). The left hand side of each plot displays the pressure (white is low pressure, black is high pressure). On the right hand side, the black particles represent those tracer particles that have been shock heated above the critical pressure for melting (~8 GPa). (A) Shows the initial model setup. (B) Shows the stage in the simulation where the shock wave has reached the back of the smaller body, and the release wave has just started to propagate from this edge. (C) Shows the release wave passing through the area of high pressure, reducing the shock pressure, and at (D) most of the high shock pressure has been released. A smaller volume of material has reached the critical shock pressure for melting than in Fig. 12.

do this, we performed Monte-Carlo simulations in which a 500 km diameter, 50% porous parent body with an initial temperature of 298 K was impacted (cratered and heated) by a population of smaller planetesimals. For each impact on the parent body we

calculated: (i) the approximate crater size on the parent body and (ii) the volume of material shock heated to several temperatures (400 K, 700 K, 1000 K, 1373 K, 2056 K). Impacts continued until an impact occurred of sufficient energy to disrupt the target body.

Impactor diameter was chosen at random from a simple power-law size–frequency distribution. The probability of an impactor being a given size or larger was given by $P(d_{imp} > d) = (d/d_{min})^{-\beta}$, where d_{min} is the diameter of the smallest impactor in the population. Results presented here are for $\beta = 1$ (i.e. as the diameter decreases by a factor of 10, the number of impactors increases by a factor of 10) and $d_{min} = 50$ m (the effect of all smaller impacts is ignored). Similarly, impact velocity was chosen at random from a Gaussian velocity–frequency distribution, with a mean (μ) of 4 km s^{-1} and a standard deviation (σ) of 1 km s^{-1}. Actual size- and velocity–frequency distributions are not well constrained and would have changed through time. The values of β, μ and σ used here were chosen to give a first-order estimate of the heating on a parent body. Future work will test the sensitivity of our model to the choice of mass- and velocity–frequency distributions.

All our numerical simulations described in the previous section assumed strengthless planetesimals and ended upon release of the colliding planetesimals from high shock pressure. As a result, the final crater dimensions were not predicted; neither was it determined whether or not the planetesimal collision resulted in disruption of both bodies. Hence, for our simple thermal evolution model we estimated crater size (D_{cr}) using the scaling law for dry sand (Schmidt and Housen, 1987):

$$D_{cr} = 1.25 g^{-0.17} d_{imp}^{0.83} v_i^{0.34}, \quad (4)$$

where g is the acceleration due to gravity on the parent body (for a 50% porous, 500 km diameter body, $g \approx 0.116$ m s^{-2}).

The disruption limit for porous small bodies is not well understood. A simple estimate of the disruption threshold for a small body greater than 10 km in diameter is provided by the largest crater diameter observed on small bodies, which is approximately equal to the radius of the body (Burchell and Leliwa-Kopystynski, 2009). For the purposes of our simple thermal evolution model we defined a disruptional impact as one that would result in a crater diameter larger than the radius of the target body; all smaller impacts were considered non-disruptional. For an impact velocity of 5 km s^{-1} and a parent body diameter of 500 km the smallest disruptional impactor diameter is 48 km.

The fraction of the parent body heated to a given temperature was estimated using an equation fit to our numerical modelling results (e.g. Fig. 10, and similar models run at different collision velocities). This equation is:

$$M(>T) = 25.7 T^{-0.81}(9.8 v_i - T^{0.50}) m_i, \quad 0 \leqslant M \leqslant m_{\text{parent}}, \quad (5)$$

where m_{parent} is the initial mass of the 500 km parent body, T is measured in Kelvin and v_i is measured in kilometres per second. This equation applies for a 50% porous parent body with an initial temperature of 298 K.

In computing the cumulative heating we assumed (crudely) that in non-disruptive collisions all heated material was retained on the parent body (i.e. no material escaped the parent body) and that each impact occurred on a pristine part of the parent body (i.e. impacts overprinting on top of one another were ignored). The first of these assumptions is supported by recent numerical simulations of impacts into porous targets with strength (Wünnemann et al., 2008).

Fig. 14 presents the combined results of many thousands of runs of the evolution model. Shown is the fraction of the parent planetesimal that is heated to several temperatures ($M(>T)/m_{\text{parent}}$) both before the final disruptive collision and after. The fractions heated to each temperature are log-normally distributed. The symbols represent the mean of the normally distributed values of $\log(M(>T)/m_{\text{parent}})$, which is approximately equivalent to the median of the normal distribution; the error bars span one standard deviation from the mean.

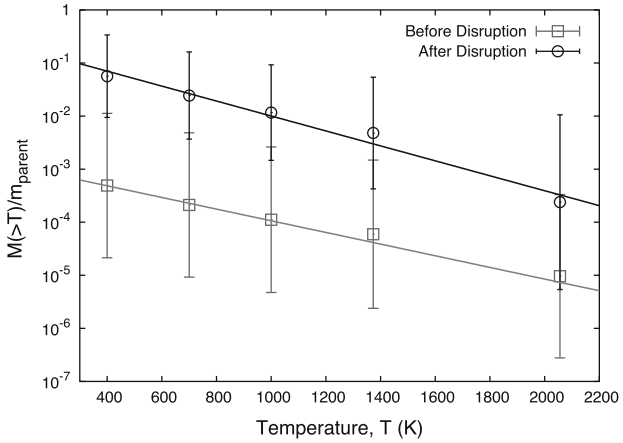

Fig. 14. The net heating of a 500 km diameter parent body before and after a disruptive collision, normalised to the initial mass of the parent body. Disruption can cause an increase of mass heated of up to two orders of magnitude, showing that most impacts will only lead to localised heating, whilst significant heating can occur during larger destructive collisions. Error bars show a 1-σ interval.

Our results show that, prior to disruption, most parent bodies are not heated significantly; the most common scenario is that less than one-thousandth of the parent body's mass is heated by 100 K, one-ten-thousandth of the parent body is heated by more than 400 K and approximately one-fifty-thousandth is melted. The standard deviations are large compared to the medians and the means are in general at least one order of magnitude greater than the medians. This implies that a small number of parent bodies will experience much more heating than is typical. However, in no scenario is more than a thirtieth of the parent body heated by greater than 100 K, more than one-eightieth heated by 400 K, or more than four thousandths of the body melted. This suggests that impacts cannot provide a mechanism for global heating of parent bodies without disrupting them; all non-disrupted parent bodies experience only volumetrically minor, highly-localised heating from collisions.

Another important result of our Monte-Carlo simulations is that the majority of heating occurs during the final, disruptive collision. In general, the disruptive collision heats about 100 times more material to a given temperature than all previous impacts put together. Hence, in most cases, almost a twentieth of the parent body is heated by more than 100 K, one-eightieth is heated by 400 K, and more than one-thousandth is melted. Again the standard deviation is large, so that a significant fraction of parent bodies are heated even more than this. For example, in about 20% of cases a third of the parent body is heated by 100 K, a tenth is heated by 400 K and a hundredth of the parent body is melted. In 8% of cases, almost the whole parent body is heated by 100 K, half of the parent body is heated by 400 K and about an eighth is melted. Hence, while planetesimals that survive without disrupting are not expected to be heated substantially by impacts, a significant proportion of the fragments produced by large collisions may be strongly heated. If planetary embryos grow primarily by accreting such fragments, rather than whole planetesimals, as recently suggested (Chambers, 2006), impact heating may play an important role in the evolution of primitive planetary materials.

Our statistical model is simplistic and a more comprehensive study is warranted. In particular, a better understanding of disruption and melt retention in porous planetesimal collisions is

required and should be incorporated in future models. A more sophisticated approach would also account for the superposition of subsequent impacts as well as the change in porosity, mass and shape of the parent body. We assumed an average impact velocity of 4 km s^{-1}. A larger impact velocity will result in more heating but will also result in disruption at a smaller impactor size. We also only considered the consequences of head-on collisions; in reality all collisions will be oblique. Previous work has shown that to a first approximation both melt production and crater volume scale with the sine of the impact angle (measured from the target surface); hence, while heating in an oblique collision will be less than in a vertical one, it will take (on average) more oblique collisions to disrupt the parent body. Therefore, we do not expect the effect of impact angle to change our conclusions. Finally, we assumed an impactor population with a power-law slope of −1. Steeper populations, with more smaller impactors and less larger ones, will result (on average) in more heating before disruption and less heating in the final disruptive collision.

The potential of impacts to heat primitive, porous Solar System material has several important implications. Relatively little heat is required to raise the temperature of volatile Solar System material above the condensation point. Hence, it is possible that during planetesimal collisions volatile elements were lost from the resulting bodies or fragments. It has also been suggested that impacts are a possible mechanism for the formation of the CB chondrules (which are younger than other chondrules and formed in a single shock event), in which melt droplets ejected from colliding bodies may cool to form chondrules (e.g., Campbell et al., 2002; Rubin et al., 2003; Krot et al., 2005). Their formation by the suggested method of a large scale impact in the early Solar System would therefore rely upon the production of melt during such a collision. The production of substantial melt volumes in single disruptive porous planetesimal collisions is predicted by our simulations. Finally, in collisions between porous planetesimals of very different sizes it is possible to generate near-surface melt (or strongly heated zones) one-to-several times larger than the smaller planetesimal. It is plausible, therefore, that parent bodies may have been heated heterogeneously, at least near the surface, from impacts of many small bodies in non-disruptive collisions. By studying the evolution of the thermal anomalies created in such impacts, a much better understanding of the chemical evolution of these primitive bodies can be gained.

Whilst the results of our simulations take a step towards quantifying the process of heating in planetesimal collisions, there are some variables not yet considered. For example, all the results presented here are for head-on collisions. In reality, all planetesimal collisions will be oblique, which can only be modelled in three dimensions. Future 3D modelling work will address this problem by studying the effect of impact angle on the efficiency of heating during planetesimal collisions. In addition, the planetesimals considered in our simulations had uniform porosity and the two planetesimals had the same porosity. Future work should also investigate the effect of layering and heterogenous pore-space distribution in planetesimals and the consequences of impacts between non-porous and highly-porous planetesimals.

Acknowledgments

This work was funded in part by NERC Grant NE/E013589/1. FJC was supported by a grant from NASA's Planetary Geology and Geophysics program. We thank Kai Wünnemann, Dirk Elbeshausen, Boris Ivanov and Jay Melosh for their help in developing iSALE. We are also grateful to Natalia Artemieva and an anonymous reviewer whose comments improved this paper.

Appendix A. Calculating the critical shock pressure for melting

To compute the critical shock pressure (and entropy) required to heat a non-porous material to a post-shock temperature T_f requires two steps. Step (1) is to compute a shock state by simultaneously solving two equations: the equation of state in the form $P = P(\rho, E)$; and the third Hugoniot equation, describing the conservation of energy during the jump from the reference state (P_0, ρ_0, E_0) to the shocked state $(P_{sh}, \rho_{sh}, E_{sh})$,

$$E_{sh} - E_0 = \frac{1}{2}(P_{sh} + P_0)\left(\frac{1}{\rho_{sh}} - \frac{1}{\rho_0}\right). \tag{6}$$

For any compressed density ρ_{sh} these two equations with two unknowns (P_{sh} and E_{sh}) can be solved. Many simple analytical equations of state are in the required form of $P = P(\rho, E)$. For equations of state that take density and temperature as independent variables, such as ANEOS, $P(\rho, E)$ must be determined implicitly from $P(\rho, T)$ and $E(\rho, T)$. Note also, that if the equation of state has provision for computing entropy and temperature, the peak shock temperature T_{sh} and entropy S_{sh} can be determined at the same time.

Step (2) is to compute the isentropic release of the material from the shock state to the final state $(P_f = P_0, E_f, \rho_f, T_f)$, which is described by the differential equation:

$$\left(\frac{\partial E}{\partial V}\right)_S = -P. \tag{7}$$

For equation of state models that include entropy and temperature, the isentropic release curve can be found using just the EoS, by iteratively searching for energy (or temperature) and density as a function of decaying pressure that maintains constant entropy. We adopt this approach using ANEOS, by solving the system of equations:

$$S = S(\rho, T) = S_{sh} \tag{8}$$

$$P = P(\rho, T) \tag{9}$$

with the initial conditions that $P = P_{sh}$, $\rho = \rho_{sh}$, $T = T_{sh}$, and the final condition that $P = P_0$.

As release from a shock state is isentropic, regardless of the initial porosity, the entropy S_{crit} required to heat the material to a given post-shock temperature T_{crit} (e.g., the solidus) is the same for all initial porosities. Hence, once S_{crit} is defined for the non-porous material (and for a given initial temperature), the critical shock pressure required to heat a porous material of the same composition to the same post-shock temperature can be computed using only the first step, above; that is, by simultaneously solving the third Hugoniot equation and the porous material equation of state $P = P(\alpha, \rho, E)$, where α, the distension, is the ratio of the solid matrix density ρ_s to the bulk density $\rho(\alpha = \rho_s/\rho)$. Distension is related to porosity ϕ by $\alpha = 1/(1 - \phi)$.

Following the approach of Carroll and Holt (1972), the pressure in a bulk porous material can be calculated from the equation of state of the solid component (where P_s is the pressure in the solid matrix) and the distension α using the thermodynamically consistent relationship:

$$P = \frac{1}{\alpha}P_s(\rho_s, E) = \frac{1}{\alpha}P_s(\alpha\rho, E). \tag{10}$$

The advantage of this formulation is that the same equation of state (tables or formulae) can be used to compute the pressure in the solid component of a porous material as in a fully-consolidated material of the same composition. The only additional requirement to compute the thermodynamic state of a porous material is to derive the distension from another state variable—the so-called compaction function.

In this work, we use a simplified version of the ϵ-α porous-compaction model (Wünnemann et al., 2006) to compute the distension from the volumetric strain ϵ:

$$\alpha = \max(1, \alpha_0 e^{\kappa\epsilon}) \tag{11}$$

where α_0 is the initial distension and κ is a control on the rate at which compaction occurs—it is a measure of how easily the pore space is compacted during compression. By convention, compressive strain is taken to be negative. $\kappa = 1$ is the idealised case of a perfectly porous material where all pore space is compacted before compression begins, and $\kappa < 1$ for materials where some compression of the solid material occurs during the compaction of the pore space. For this study we assumed $\kappa = 0.98$, which has proven to give good fits to Hugoniot data for a range of geologic materials and initial porosities (Wünnemann et al., 2006, 2008). The sensitivity of our results to the choice of κ is discussed in the text.

From the definition of volumetric strain $\epsilon = \ln(\rho_0/\rho)$, distension can be related directly to the density of the porous material

$$\alpha = \max\left(1, \alpha_0 \left(\frac{\rho_0}{\rho}\right)^{\kappa}\right). \tag{12}$$

Hence, in the case of a porous material, for any compressed density ρ_{sh}, the three Eqs. (6), (10) and (12), with three unknowns (α_{sh}, P_{sh} and E_{sh}), can be solved to define the shock state. The critical shock pressure required to heat a porous material to a given post-shock temperature is then the shock pressure P_{sh} at which the entropy is equal to the critical entropy, $S_{sh} = S_{crit}$.

References

Ahrens, T.J., Cole, D.M., 1974. Shock compression and adiabatic release of lunar fines from Apollo 17. Proc. Lunar Sci. Conf. 5, 2333–2345.

Ahrens, T.J., O'Keefe, J.D., 1977. Equations of state and impact-induced shock-wave attenuation on the Moon. In: Roddy, D.J., Pepin, R.O., Merrill, R.B. (Eds.), Impact and Explosion Cratering: Planetary and Terrestrial Implications. pp. 639–656.

Amsden, A., Ruppel, H., Hirt, C., 1980. SALE: A simplified ALE Computer Program for Fluid Flow at all Speeds. Los Alamos National Laboratories Report LA-8095, Los Alamos, New Mexico: LANL, 101p.

Bauer, J., 1979. Expermental shock metamorphism of mono- and polycrystalline olivine: A comparative study. Proc. Lunar Sci. Conf. 10, 2573–2596.

Benz, W., Cameron, A.G.W., Melosh, H.J., 1989. The origin of the Moon and the single-impact hypothesis III. Icarus 81, 113–131.

Bjorkman, M.D., Holsapple, K.A., 1987. Velocity scaling impact melt volume. Int. J. Impact Eng. 5, 155–163.

Blum, J., 2003. The structure of planetesimals in the solar nebula. Meteorit. Planet. Sci. Suppl. 38, 5152 (abstracts).

Bottke Jr., W.F., Durda, D.D., Nesvorný, D., Jedicke, R., Morbidelli, A., Vokrouhlický, D., Levison, H.F., 2005. Linking the collisional history of the main asteroid belt to its dynamical excitation and depletion. Icarus 179 (1), 63–94.

Britt, D.T., Yeomans, D., Housen, K., Consolmagno, G., 2002. Asteroid density, porosity, and structure. In: Bottke, W.F., Jr., Cellino, A., Paolicchi, P., Binzel, R.P. (Eds.), Asteroids III. University of Arizona Press, Tucson, pp. 485–500.

Burchell, M.J., Leliwa-Kopystynski, J., 2009. The large crater on Asteroid Steins: Is it abnormally large? Lunar Planet. Sci. 40, 1525 (abstracts).

Cameron, A.G.W., Benz, W., Wasson, J.T., 1990. Heating during asteroidal collisions. Lunar Planet. Inst. 21, 155–156 (abstracts).

Cameron, A.G.W., Benz, W., Wasson, J.T., 1991. Heating during asteroidal collisions II. Lunar Planet. Inst. Conf. 22, 173–174 (abstracts).

Campbell, A.J., Humayun, M., Weisberg, M.K., 2002. Siderophile element constraints on the formation of metal in the metal-rich chondrites Bencubbin, Weatherford, and Gujba. Geochim. Cosmochim. Acta 66 (4), 647–660.

Carroll, M.M., Holt, A.C., 1972. Static and dynamic pore-collapse relations for ductile porous materials. J. Appl. Phys. 43 (4), 1626–1636.

Cassen, P., 1994. Utilitarian models of the solar nebula. Icarus 112, 405–429.

Chambers, J., 2006. A semi-analytic model for oligarchic growth. Icarus 180, 496–513.

Chao, E.C.T., 1967. Shock effects in certain rock-forming minerals. Science 156, 192–202.

Chao, E.C.T., 1968. Pressure and temperature history of impact metamorphosed rocks based on petrographic observations. In: French, B.M., Short, N.M. (Eds.), Shock Metamorphism of Natural Materials, Mono, Baltimore, pp. 135–158.

Collins, G.S., Melosh, H.J., Ivanov, B.A., 2004. Modeling damage and deformation in impact simulations. Meteorit. Planet. Sci. 39, 217–231.

Consolmagno, G., Britt, D., 2004. Meteoritical evidence and constraints on asteroid impacts and disruption. Planet. Space Sci. 52, 1119–1128.

Cuzzi, J.N., Hogan, R.C., Shariff, K., 2008. Toward planetesimals: Dense chondrule clumps in the protoplanetary nebula. Astrophys. J. 687, 1432–1447.

Dominik, C., Tielens, A.G.G.M., 1997. The physics of dust coagulation and the structure of dust aggregates in space. Astrophys. J. 480, 647–673.

Ghosh, A., Weidenschilling, S.J., McSween Jr., H.Y., Rubin, A., 2006. Asteroidal heating and thermal stratification of the asteroid belt. In: Lauretta, D.S., McSween, H.Y., Jr. (Eds.), Meteorites and the Early Solar System II. University of Arizona Press, Tucson, pp. 555–566.

Herbert, F., 1989. Primordial electrical induction heating of asteroids. Icarus 78, 402–410.

Hörz, F., Cintala, M., See, T., Loan, L., 2005. Shock melting of ordinary chondrite powders and implications for asteroidal regoliths. Meteorit. Planet. Sci. 40, 1329–1346.

Hörz, F., Schaal, R.B., 1981. Asteroidal agglutinate formation and implications for asteroidal surfaces. Icarus 46, 337–353.

Huffman, A., Reimold, W., 1996. Experimental constraints on shock-induced microstructures in naturally deformed silicates. Tectonophysics 256, 165–217.

Ivanov, B., 2005. Numerical modeling of the largest terrestrial meteorite craters. Solar Syst. Res. 39 (5), 381–409.

Ivanov, B.A., Artemieva, N.A., 2002. Numerical Modeling of the Formation of Large Impact Craters. Special Paper 356: Catastrophic Events and Mass Extinctions: Impacts and Beyond 356, pp. 619–630.

Ivanov, B.A., Deniem, D., Neukum, G., 1997. Implementation of dynamic strength models into 2D hydrocodes: Applications for atmospheric breakup and impact cratering. Int. J. Impact Eng. 20, 411–430.

Johansen, A., Oishi, J.S., Low, M.-M.M., Klahr, H., Henning, T., Youdin, A., 2007. Rapid planetesimal formation in turbulent circumstellar disks. Nature 448, 1022–1025.

Jutzi, M., Benz, W., Michel, P., 2008. Numerical simulations of impacts involving porous bodies: I. Implementing sub-resolution porosity in a 3D SPH hydrocode. Icarus 198 (1), 242–255.

Katz, R.F., Spiegelman, M., Langmuir, C.H., 2003. A new parameterization of hydrous mantle melting. Geochem. Geophys. Geosyst. 4. Article no. 1073.

Keil, K., Stöffler, D., Love, S., Scott, E., 1997. Constraints on the role of impact heating and melting in asteroids. Meteorit. Planet. Sci. 32, 349–363.

Kenyon, S.J., Bromley, B.C., 2001. Gravitational stirring in planetary debris disks. Astron. J. 121, 538–551.

Kieffer, S.W., 1971. Shock metamorphism of the Coconino sandstone at meteor crater, Arizona. J. Geophys. Res. 76, 5449–5473.

Kieffer, S.W., Phakey, P.P., Christie, M.J., 1976. Shock processes in porous quartzite: transmission electron microscope observations and theory. Contrib. Mineral. Petrol. 59, 41–93.

Krot, A.N., Amelin, Y., Cassen, P., Meibom, A., 2005. Young chondrules in CB chondrites from a giant impact in the early Solar System. Nature 436 (7053), 989–992.

Lee, T., Papanastassiou, D.A., Wasserburg, G.J., 1976. Demonstration of ^{26}Mg excess in Allende and evidence for ^{26}Al. Geophys. Res. Lett. 3, 41–44.

Love, S.G., Ahrens, T.J., 1996. Catastrophic impacts on gravity dominated asteroids. Icarus 124, 141–155.

Love, S.G., Hörz, F., Brownlee, D.E., 1993. Target porosity effects in impact cratering and collisional disruption. Icarus 105, 216–224.

MacPherson, G.J., Davis, A.M., Zinner, E.K., 1995. The distribution of aluminum-26 in the early Solar System – A reappraisal. Meteoritics 30, 365–386.

McKenzie, D., Bickle, M., 1988. The volume and composition of melt generated by extension of the lithosphere. J. Petrol. 29 (Part 1), 625–679.

McSween, H.J., Ghosh, A., Grimm, R.E., Wilson, L., Young, E.D., 2002. Thermal evolution models of asteroids. In: Bottke, W.F., Jr., Cellino, A., Paolicchi, P., Binzel, R.P. (Eds.), Asteroids III. University of Arizona Press, Tucson, pp. 559–571.

Melosh, H.J., 1989. Impact Cratering: A Geologic Process. Oxford University Press, New York. 245p.

Melosh, H.J., 2007. A hydrocode equation of state for SiO_2. Meteorit. Planet. Sci. 42, 2079–2098.

Melosh, H.J., Ryan, E.V., Asphaug, E., 1992. Dynamic fragmentation in impacts: Hydrocode simulation of laboratory impacts. J. Geophys. Res. 97, 14735–14759.

Morbidelli, A., Bottke, W.F., Nesvorný, D., Levison, H.F., 2009. Asteroids were born big. Icarus 204, 558–573.

Pierazzo, E., and 13 colleagues, 2008. Validation of numerical codes for impact and explosion cratering: Impacts on strengthless and metal targets. Meteorit. Planet. Sci. 43 (12), 1917–1938.

Pierazzo, E., Melosh, H.J., 2000. Melt production in oblique impacts. Icarus 145, 252–261.

Pierazzo, E., Vickery, A.M., Melosh, H.J., 1997. A reevaluation of impact melt production. Icarus 127, 408–423.

Reimold, W.U., Stoeffler, D., 1978. Experimental shock metamorphism of dunite. Proc. Lunar Sci. Conf. 9, 2805–2824.

Rubin, A., 1995. Petrological evidence for collisional heating of chondritic asteroids. Icarus 113, 156–167.

Rubin, A.E., Kallemeyn, G.W., Wasson, J.T., Clayton, R.N., Mayeda, T.K., Grady, M., Verchovsky, A.B., Eugster, O., Lorenzetti, S., 2003. Formation of metal and silicate globules in Gujba: A new Bencubbin-like meteorite fall. Geochim. Cosmochim. Acta 67 (17), 3283–3298.

Russell, S.S., Srinivasan, G., Huss, G.R., Wasserburg, G.J., MacPherson, G.J., 1996. Evidence for widespread ^{26}Al in the solar nebula and constraints for nebula time scales. Science 273, 757–762.

Schmidt, R.M., Housen, K.R., 1987. Some recent advances in the scaling of impact and explosion cratering. Int. J. Impact Eng. 5, 543–560.

Schmitt, R.T., 2000. Shock experiments with the H6 chondrite Kernouvé: Pressure calibration of microscopic shock effects. Meteorit. Planet. Sci. 35, 545–560.
Scott, E., 2002. Meteorite evidence for the accretion and collisional evolution of asteroids. In: Bottke, W.F., Jr., Cellino, A., Paolicchi, P., Binzel, R.P. (Eds.), Asteroids III. University of Arizona Press, Tucson, pp. 697–709.
Scott, E.R.D., Keil, K., Stöffler, D., 1992. Shock metamorphism of carbonaceous chondrites. Geochim. Cosmochim. Acta 56 (12), 4281–4293.
Sharp, T., de Carli, P., 2006. Shock effects in meteorites. In: Lauretta, D.S., McSween, H.Y., Jr. (Eds.), Meteorites and the Early Solar System II. University of Arizona Press, Tucson, pp. 653–677.
Sonett, C., Colburn, D., Schwartz, K., 1968. Electrical heating of meteorite parent bodies and planets by dynamo induction from a pre-main sequence T Tauri 'Solar Wind'. Nature 219, 924–926.
Srinivasan, G., Goswami, J.N., Bhandari, N., 1999. ^{26}Al in Eucrite Piplia Kalan: Plausible heat source and formation chronology. Science 284, 1348–1350.
Stöffler, D., Keil, K., Scott, E.R.D., 1991. Shock metamorphism of ordinary chondrites. Geochim. Cosmochim. Acta 55, 3845–3867.
Thompson, S., Lauson, H., 1972. Improvements in the CHART D Radiation-hydrodynamic Code III: Revised Analytic Equations of State. Sandia National Laboratory Report SC-RR-71 0714, 113p.
Urey, H., 1955. The cosmic abundances of potassium, uranium, and thorium and the heat balances of the Earth, the Moon and Mars. Proc. Natl. Acad. Sci. 41, 127–144.
Wasson, J.T., Rubin, A.E., Benz, W., 1987. Heating of primitive, asteroid-size bodies by large impacts. Meteoritics 22, 525–526.
Weidenschilling, S., Davis, D., Marzari, F., 2001. Very early collisional evolution of the asteroid belt. Earth Planets Space 53, 1093–1097.
Weidenschilling, S., Marzari, F., Hood, L., 1998. The origin of chondrules at jovian resonances. Science 279, 681–684.
Weidenschilling, S.J., 1977. The distribution of mass in the planetary system and solar nebula. Astrophys. Space Sci. 51 (1), 153–158.
Weidenschilling, S.J., 2009. How big were the first planetesimals? Does size matter? Lunar Planet. Inst. Sci. Conf. 40, 1760 (abstract).
Wetherill, G.W., Stewart, G.R., 1989. Accumulation of a swarm of small planetesimals. Icarus 77, 330–357.
Wünnemann, K., Collins, G., Melosh, H., 2006. A strain-based porosity model for use in hydrocode simulations of impacts and implications for transient crater growth in porous targets. Icarus 180, 514–527.
Wünnemann, K., Collins, G., Osinski, G., 2008. Numerical modelling of impact melt production in porous rocks. Earth Planet. Sci. Lett. 269 (3–4), 529–538.
Wurm, G., Blum, J., Colwell, J.E., 2001. Aerodynamical sticking of dust aggregates. Phys. Rev. E 64 (4). Article no. 046301.
Wurm, G., Paraskov, G., Krauss, O., 2004. On the importance of gas flow through porous bodies for the formation of planetesimals. Astrophys. J. 606 (2), 983–987.
Zel'Dovich, Y.B., Raizer, Y.P., 1967. Physics of Shock Waves and High-temperature Hydrodynamic Phenomena, vol. 2. Dover Publications, Mineola, NY. pp. 712–716 (Chapter 11).